AIAA JOURNAL
Vol. 38, No. 2, February 2000

Dynamic Stability of Rectangular Plates Subjected to Pulsating Follower Forces

Youn-Sun Choo*
Agency for Defense Development, Taejeon 305-600, Republic of Korea
and
Ji-Hwan Kim†
Seoul National University, Seoul 151-742, Republic of Korea

The dynamic stability of isotropic and nonsymmetric laminated plates with four free edges subjected to pulsating follower forces is discussed. The results are obtained using the first-order shear deformation theory. The discretized equation of motion is obtained by the finite element method, and then the method of multiple scales is adopted to investigate the dynamic instability regions. The effects of Poisson ratio as well as aspect and thickness ratios on the dynamic instability region for isotropic plates are investigated. The influences of aspect ratio, lamination angle, and the number of layers for nonsymmetric, cross-ply, and angle-ply laminated plates are also studied.

Introduction

In general, forces acting on a structure can be divided into conservative forces and nonconservative forces. The follower force is a typical example of a nonconservative force. When a structure is under a constant follower force whose direction changes according to the deformation of the structure, it may undergo the static instability (divergence) such that transverse natural frequencies merge into zero or the dynamic instability (flutter) such that two natural frequencies coincide with each other, and so the amplitude of vibration grows without bound. Examples of structures subjected to follower forces include missiles, rockets, and space vehicles changing orbit under thrust.

Many researchers have studied the stability of a free-free beam under follower forces. Beal[1] considered the beam as a simple model of a missile or rocket and analyzed the stability characteristics of the beam under constant or pulsating follower forces. The effects of gain, location of control sensor, and concentrated mass were also investigated.[2–5] Higuchi and Dowell[6,7] examined, by modal analysis, the instability phenomena of a completely free-edged plate, neglecting the rotary inertia and shear deformation due to constant follower forces. It was shown that critical forces are sensitive to the variation of aspect and Poisson ratios.

When a beam or a plate is exposed to an axial or in-plane pulsating force not greater than a critical value, they, respectively, experience an axial or in-plane vibration only. However, if certain conditions are satisfied between driving and transverse natural frequencies, then the dynamic instability called "parametric resonance" occurs and the amplitude of transverse vibration increases without bound. This kind of instability phenomenon, appearing for a plate under pulsating forces, was also studied in the literature. Hutty et al.[8] examined the dynamic stability of a thin plate subjected to pulsating compressive and shear loads. Duffield and Willems[9] compared numerical and experimental results for a stiffened rectangular plate with periodic loads to see the effects of stiffeners. Existing results reveal that pulsating forces also affect the stability of aerospace structures. Young and Chen[10,11] studied, using the method of multiple scales, a cantilevered skew plate on which aerodynamic and harmonic in-plane forces acted simultaneously. It was shown in their work that even the in-plane force smaller than the aerodynamic force can cause the system to be unstable before the latter reaches its critical value. Also, it was found that the harmonic in-plane force may act so that the system remains stable at certain combinations of the exciting frequencies and amplitudes even if the aerodynamic force exceeds the critical value.

Composite materials are now widely employed in aerospace structures because high strength and/or stiffness is obtainable without increasing the weight. As a result, much attention has been given to the dynamic stability of laminated plates. Srinivasan[12] examined the stability of a thin laminated plate applying the finite strip method and Bolotin's method. Chen and Yang[13] investigated a nonsymmetric plate under both periodic compressive stress and bending stress, and showed that the increase in bending stress leads to the expansion of the instability region. Cederbaum[14] applied first-order and high-order shear deformation theories to a nonsymmetric laminated plate and concluded that the two theories give almost the same results. Liao and Cheng[15] utilized the finite element method to study the instability region of a stiffened laminated plate and shell subjected to pulsating in-plane forces. They analyzed the effects of skew angle, lamination scheme, and curvature of the cylindrical shell on the instability region.

In most of the works just mentioned, the focus was placed on the systems under periodic forces that were not of the follower type (exceptions are Refs. 11 and 15, where some numerical results for follower-type forces are presented). This paper discusses the dynamic stability of isotropic or nonsymmetric laminated rectangular plates with four free edges subjected to pulsating follower forces. The results are obtained using the first-order shear deformation theory. The discretized equation of motion is obtained by the finite element method, and then the method of multiple scales is adopted to investigate the dynamic instability region. The effects of the Poisson ratio as well as aspect and thickness ratios in the dynamic instability region for isotropic plates are investigated. The influences of aspect ratio, lamination angle, and the number of plys for nonsymmetric cross-ply and angle-ply laminated plates are also studied.

Theory

Consider a completely free-edged rectangular plate with side length $a \times b$ and thickness h subjected to uniformly distributed pulsating follower forces $P_0 + P_1 \cos \Omega t$ as shown in Fig. 1, where P_0 and P_1 are the magnitudes of constant and time-varying forces, respectively, and Ω is the driving frequency of the time-varying force.

Energy Equation of Isotropic Plate

Let u_1, u_2, and u_3 be the displacements of the plate in the x, y, and z directions, respectively. Then the displacement field of the plate taking into account the shear deformation at an arbitrary point takes the form

Received 28 July 1998; revision received 22 June 1999; accepted for publication 23 July 1999.

*Researcher, P.O. Box 35-3, Yuseong.
†Associate Professor, Department of Aerospace Engineering. Member AIAA.

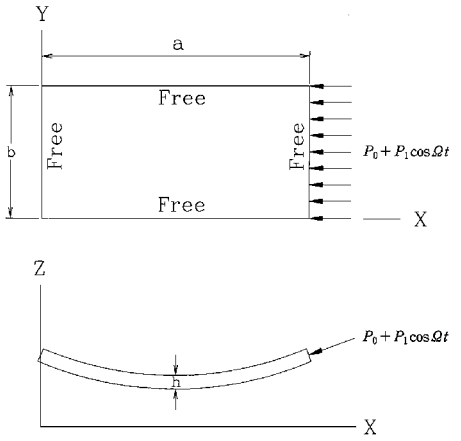

Fig. 1 Rectangular plate with four free edges subjected to pulsating follower forces.

$$u_1(x, y, z, t) = u(x, y, t) - z\psi_x(x, y, t)$$
$$u_2(x, y, z, t) = v(x, y, t) - z\psi_y(x, y, t)$$
$$u_3(x, y, z, t) = w(x, y, t) \tag{1}$$

where u, v, and w denote the displacements of a point (x, y) on the midplane and ψ_x and ψ_y are the rotations of line elements perpendicular to the midplane about the y and x axes, respectively. For the isotropic plate, no coupling exists between in-plane and out-of-plane displacements. Then, neglecting the in-plane displacements effect on the midplane, Eq. (1) can be written as

$$u_1(x, y, z, t) = -z\psi_x(x, y, t), \qquad u_2(x, y, z, t) = -z\psi_y(x, y, t)$$
$$u_3(x, y, z, t) = w(x, y, t) \tag{2}$$

For the displacement field given in Eq. (2), the kinetic and strain energies considering rotary inertia and shear deformation are given by

$$T = \frac{1}{2}\int_R \left\{\rho h\dot{w}^2 + \frac{1}{12}\rho h^3\dot{\psi}_x^2 + \frac{1}{12}\rho h^3\dot{\psi}_y^2\right\} dA \tag{3}$$

$$U = \frac{1}{2}\int_R \left[D(\psi_{x,x}^2 + \psi_{y,y}^2 + 2\nu\psi_{x,x}\psi_{y,y}) + \frac{Gh^3}{12}(\psi_{x,y} + \psi_{y,x})^2 + khG\{(w_{,x} - \psi_x)^2 + (w_{,y} - \psi_y)^2\}\right] dA \tag{4}$$

where $\dot{(\cdot)} = d(\cdot)/dt$, $(\cdot)_{,\beta} = \partial(\cdot)/\partial\beta$, $(\beta = x$ or $y)$, D is the bending rigidity of the plate, G is the shear modulus, k is the shear correction factor having the value of $\frac{5}{6}$ for rectangular cross sections, R is area, and $dA = dx\, dy$.

Energy Equation of Laminated Composite Plate

Whereas the displacement field of the symmetric laminated plate is given by Eq. (2), the expression given by Eq. (1) should be used for the nonsymmetric laminated composite plate because the in-plane displacements are coupled to the out-of-plane displacements. As a result, the strains are given by

$$\begin{pmatrix}\varepsilon_x\\ \varepsilon_y\\ \gamma_{xy}\end{pmatrix} = \begin{pmatrix}u_{,x}\\ v_{,y}\\ u_{,y} + v_{,x}\end{pmatrix} - z\begin{pmatrix}\psi_{x,x}\\ \psi_{y,y}\\ \psi_{x,y} + \psi_{y,x}\end{pmatrix} = \varepsilon_o + z\chi \tag{5a}$$

$$\begin{pmatrix}\gamma_{yz}\\ \gamma_{xz}\end{pmatrix} = \begin{pmatrix}w_{,y} - \psi_y\\ w_{,x} - \psi_x\end{pmatrix} = \varepsilon_s \tag{5b}$$

where ε_o, χ, and ε_s, respectively, denote the in-plane strain vector, bending curvature vector, and transverse shear strain vector. Note that the transverse normal strain is neglected in Eqs. (5a) and (5b).

The in-plane and out-of-plane stresses in the kth lamina are given by

$$\sigma_k = \begin{pmatrix}\sigma_x\\ \sigma_y\\ \sigma_{xy}\end{pmatrix}_k = [\bar{Q}_{ij}^{(k)}]\begin{pmatrix}\varepsilon_x\\ \varepsilon_y\\ \varepsilon_{xy}\end{pmatrix}_k = [\bar{Q}_{ij}^{(k)}]\{\varepsilon_{o(k)} + z\chi_{(k)}\} \tag{6a}$$

$$\tau_k = \begin{pmatrix}\tau_{yz}\\ \tau_{xz}\end{pmatrix}_k = \begin{bmatrix}\bar{Q}_{44}^{(k)} & \bar{Q}_{45}^{(k)}\\ \bar{Q}_{45}^{(k)} & \bar{Q}_{55}^{(k)}\end{bmatrix}\begin{pmatrix}\gamma_{yz}\\ \gamma_{xz}\end{pmatrix}_k = \begin{bmatrix}\bar{Q}_{44}^{(k)} & \bar{Q}_{45}^{(k)}\\ \bar{Q}_{45}^{(k)} & \bar{Q}_{55}^{(k)}\end{bmatrix}\varepsilon_s \tag{6b}$$

where $\bar{Q}_{ij}^{(k)}$ denotes the plane stress reduced elastic constants of the kth layer oriented at an arbitrary angle θ_k with respect to the plate coordinate axes.

Employing the following equations to derive the stress and moment resultants:

$$(N_i, M_i) = \int_{-h/2}^{h/2} \sigma_i(1, z)\, dz, \qquad (i = 1, 2, 6)$$
$$(Q_1, Q_2) = \int_{-h/2}^{h/2} (\sigma_5, \sigma_4)\, dz \tag{7}$$

we obtain the constitutive equations

$$\boldsymbol{N} = \begin{pmatrix}N_x\\ N_y\\ N_{xy}\end{pmatrix} = \int_{-h/2}^{h/2}\begin{pmatrix}\sigma_x\\ \sigma_y\\ \sigma_{xy}\end{pmatrix} dz = \sum_{k=1}^{N}\int_{z_{k-1}}^{z_k}\begin{pmatrix}\sigma_x\\ \sigma_y\\ \sigma_{xy}\end{pmatrix}_k dz$$
$$= [A_{ij}]\varepsilon_o + [B_{ij}]\chi = \boldsymbol{A}\varepsilon_o + \boldsymbol{B}\chi \tag{8a}$$

$$\boldsymbol{M} = \begin{pmatrix}M_x\\ M_y\\ M_{xy}\end{pmatrix} = \int_{-h/2}^{h/2}\begin{pmatrix}\sigma_x\\ \sigma_y\\ \sigma_{xy}\end{pmatrix} z\, dz = \sum_{k=1}^{N}\int_{z_{k-1}}^{z_k}\begin{pmatrix}\sigma_x\\ \sigma_y\\ \sigma_{xy}\end{pmatrix}_k z\, dz$$
$$= [B_{ij}]\varepsilon_o + [D_{ij}]\chi = \boldsymbol{B}\varepsilon_o + \boldsymbol{D}\chi \tag{8b}$$

$$\boldsymbol{Q} = \begin{pmatrix}Q_y\\ Q_x\end{pmatrix} = \int_{-h/2}^{h/2}\begin{pmatrix}\tau_{yz}\\ \tau_{xz}\end{pmatrix} dz = \sum_{k=1}^{N}\int_{z_{k-1}}^{z_k}\begin{pmatrix}\tau_{yz}\\ \tau_{xz}\end{pmatrix}_k dz$$
$$= [A_{ij}]\varepsilon_s = \boldsymbol{A}_s\varepsilon_s \tag{8c}$$

where N is the number of layers in the laminate,

$$(A_{ij}, B_{ij}, D_{ij}) = \sum_{k=1}^{N}\int_{z_{k-1}}^{z_k}(1, z, z^2)\bar{Q}_{ij}^{(k)}\, dz \qquad (i = 1, 2, 6)$$
$$A_{ij} = \sum_{k=1}^{N} k_i k_j \int_{z_{k-1}}^{z_k}\bar{Q}_{ij}^{(k)}\, dz \qquad (i, j = 4, 5)$$

are the stiffness coefficients, and k_i $(i = 4, 5)$ is the shear correction coefficient.

The kinetic energy T and the strain energy U of homogeneous laminated plate are in general expressed by

$$T = \frac{1}{2}\int_V \rho(\dot{u}_1^2 + \dot{u}_2^2 + \dot{u}_3^2)\, dV$$
$$= \frac{1}{2}\int_R \left[I_0(\dot{u}^2 + \dot{v}^2 + \dot{w}^2) + I_2(\dot{\psi}_x^2 + \dot{\psi}_y^2)\right] dA \tag{9}$$

$$U = \frac{1}{2}\int_V (\sigma_x\varepsilon_x + \sigma_y\varepsilon_y + \tau_{yz}\gamma_{yz} + \tau_{xz}\gamma_{xz} + \tau_{xy}\gamma_{xy})\, dV$$
$$= \frac{1}{2}\int_R \left[\int_{-h/2}^{h/2}\{(\varepsilon^T\sigma_k + \varepsilon_s^T\tau_k)\}\, dz\right] dA$$
$$= \frac{1}{2}\int_R (\varepsilon_o^T\boldsymbol{N} + \chi^T\boldsymbol{N} + \varepsilon_s^T\boldsymbol{Q})\, dA \tag{10}$$

where V is volume,

$$(I_0, I_2) = \int_{-h/2}^{h/2} \rho(1, z^2)\,\mathrm{d}z = \sum_{k=1}^{N} \int_{z_{k-1}}^{z_k} \rho(1, z^2)\,\mathrm{d}z$$

respectively, denote the translational and rotational inertia coefficients, and ρ is the material density.

External Work

The compressive in-plane force acting on the cross section of the free-edged plate shown in Fig. 1 varies linearly along the x axis due to the inertia force. Then the external work W_c done by the in-plane components of the follower force is expressed by

$$W_c = \frac{1}{2}\int_R (P_0 + P_1 \cos \Omega t)\frac{x}{a} w_{,x}^2\,\mathrm{d}A \tag{11}$$

On the other hand, the virtual external work due to the vertical components of the follower force is given by

$$\delta W_{nc} = -\int_R (P_0 + P_1 \cos \Omega t) w_{,x} \bar{\delta}(x - a)\delta w\,\mathrm{d}A \tag{12}$$

where $\bar{\delta}(x - a)$ is the Dirac's delta function.

Formulation

For the equations derived, Hamilton's principle can be expressed by

$$\delta \int_{t_1}^{t_2} (T - U + W_c)\,\mathrm{d}t + \int_{t_1}^{t_2} \delta W_{nc}\,\mathrm{d}t = 0 \tag{13}$$

To discretize the equation of motion obtained by Hamilton's principle, we employ the finite element method using a 16-node Lagrange element. The degrees of freedom at a node are three for an isotropic plate or five for a composite plate, respectively, and the shape functions are seen in Ref. 16.

Applying Hamilton's principle and the finite element method, we obtain the following discretized equation of motion:

$$\boldsymbol{M}\{\ddot{u}\} + [\boldsymbol{K}_e - \alpha P_{\mathrm{cr}} \boldsymbol{K}_{g_s}]\{u\} - [\beta P_{\mathrm{cr}} \boldsymbol{K}_{g_t} \cos \Omega t]\{u\} = 0 \tag{14}$$

where $\alpha = P_0/P_{\mathrm{cr}}$, $\beta = P_1/P_{\mathrm{cr}}$, P_{cr} is the critical force that induces flutter or divergence at each case under constant follower forces, $\{u\}$ is the n-dimensional vector of the plate, $\boldsymbol{M}$ is the mass matrix, $\boldsymbol{K}_e$ is the elastic stiffness matrix, and K_{g_s} and $\boldsymbol{K}_{g_t}$, respectively, denote the geometric stiffness matrices due to constant and time-varying follower forces. If, as in this paper, constant and time-varying forces are applied in the same way, then we have $\boldsymbol{K}_g = \boldsymbol{K}_{g_s} = \boldsymbol{K}_{g_t}$. Let $\boldsymbol{K} = \boldsymbol{K}_e - \alpha P_{\mathrm{cr}} \boldsymbol{K}_g$ and rewrite Eq. (14) as

$$\boldsymbol{M}\{\ddot{u}\} + \boldsymbol{K}\{u\} - \beta P_{\mathrm{cr}} \cos \Omega t\, \boldsymbol{K}_g\{u\} = 0 \tag{15}$$

Note that $\boldsymbol{K}$ is a nonsymmetric matrix due to the nonconservative forces.

We now transform $\boldsymbol{M}$ and $\boldsymbol{K}$ into diagonal matrices using modal transformation. In general, one rigid-body translation mode and two rigid-body rotation modes appear for a completely free-edged isotropic plate, whereas three translation and three rotation modes are observed for a composite plate. We assume that such rigid-body modes are controlled by proper control systems.[6] To exclude the effect of rigid-body modes, modal vectors related to only elastic vibration modes are used in the transformation. Let $\boldsymbol{\Phi}$ and $\boldsymbol{\Psi}$ be the $n \times (n - p)$ normalized right and left modal matrices, respectively, and let p be the number of rigid body modes. By the substitution the transformation $\{u\} = \boldsymbol{\Phi}\{\eta\}$ and premultiplying by $\boldsymbol{\Psi}^T$ on both sides, Eq. (15) leads to the following equation of motion:

$$\boldsymbol{I}\{\ddot{\eta}\} + \boldsymbol{\Lambda}\{\eta\} - \beta P_{\mathrm{cr}} \cos \Omega t\, \boldsymbol{R}\{\eta\} = 0 \tag{16}$$

with $\boldsymbol{\Psi}^T \boldsymbol{M} \boldsymbol{\Phi} = \boldsymbol{I}$, $\boldsymbol{\Psi}^T \boldsymbol{K} \boldsymbol{\Phi} = \boldsymbol{\Lambda}$, $\boldsymbol{\Psi}^T \boldsymbol{K}_g \boldsymbol{\Phi} = \boldsymbol{R}$, and where $\boldsymbol{I}$ is the identity matrix. Note that the diagonal entries of $\boldsymbol{\Lambda}$ are just the squares, w_i^2, $1 \le i \le n - p$, of the natural frequencies of the plate under the constant follower force. Rewriting Eq. (16) in component form, we have

$$\ddot{\eta}_j + \omega_j^2 \eta_j + 2\varepsilon \cos \Omega t \sum_{m=1}^{n-p} \tilde{R}_{jm} \eta_m = 0, \qquad j = 1, 2, \ldots, n - p \tag{17}$$

where $\varepsilon = -\beta/2$ and $\tilde{R}_{jm} = R_{jm} P_{\mathrm{cr}}$. According to the method of multiple scales, the solutions of Eqs. (17) can be expressed by a series expansion of ε as follows[17]:

$$\eta_j(t, \varepsilon) = \sum_{m=0}^{\infty} \varepsilon^m \eta_{jm}(T_0, T_1, T_2, \ldots), \qquad j = 1, 2, \ldots, n - p \tag{18}$$

where $T_n = \varepsilon^n t$, and $n = 0, 1, 2, \ldots$.

Through the first-order approximation [i.e., by considering the first two terms only in Eqs. (18)], we can define transition curves that separate stable solutions from unstable ones in the $\varepsilon - \Omega$ plane by (see Ref. 17 for details) 1) $\Omega \simeq \omega_p + \omega_q$ (sum-type, combination resonance), which gives us

$$\Omega = \omega_q + \omega_p \pm \varepsilon \left[\frac{\tilde{R}_{pq}\tilde{R}_{qp}}{\omega_p \omega_q}\right]^{\frac{1}{2}} + O(\varepsilon^2) \tag{19a}$$

and 2) $\Omega \simeq \omega_q - \omega_p$ (difference-type, combination resonance), which gives us

$$\Omega = \omega_q - \omega_p \pm \varepsilon \left[-\frac{\tilde{R}_{pq}\tilde{R}_{qp}}{\omega_p \omega_q}\right]^{\frac{1}{2}} + O(\varepsilon^2) \tag{19b}$$

From Eqs. (19a) and (19b), it is easily seen that the sum-type and difference-type combination resonances cannot exist simultaneously for any pair of natural frequencies ω_p and ω_q. Furthermore, if a force is of constant direction type, then the difference-typecombination resonance does not appear due to the symmetry of $\boldsymbol{R}$. For a follower force, however, $\tilde{R}_{pq}$ and $\tilde{R}_{qp}$ can have opposite signs and so the difference type may also exist.

Numerical Results and Discussion

Based on the formulations in the preceding section, we now analyze the dynamic stability of the plates under pulsating follower forces. For the numerical calculations, the following nondimensional quantities are defined as follows.

For isotropic plates, $\bar{\omega} = \omega a^2 \sqrt{(\rho h/D)}$, $\bar{\Omega} = \Omega a^2 \sqrt{(\rho h/D)}$, and $\bar{P}_{\mathrm{cr}} = P_{\mathrm{cr}} a^2/D$, and for composite plates, $\bar{\omega} = \omega a^2 \sqrt{[\rho/(E_2 h^2)]}$, $\bar{\Omega} = \Omega a^2 \sqrt{[\rho/(E_2 h^2)]}$, and $\bar{P}_{\mathrm{cr}} = P_{\mathrm{cr}} a^2/(E_2 h^3)$, where $\bar{\omega}$ is the nondimensional natural frequency, $\bar{\Omega}$ is the nondimensional driving frequency, and $\bar{P}_{\mathrm{cr}}$ is the nondimensional critical force.

First, we check the validity of the finite element code used in our numerical studies. For isotropic plates the critical forces are compared with that of Ref. 7. Because the results of Ref. 7 were obtained for thin plates, the critical forces for the thickness ratio of $\frac{1}{100}$ were used for comparison for which the effects of rotary inertia and shear deformation rarely appear in the Mindlin's theory of plate. Table 1 contains the comparative results. The critical force of the code with 4×4 plate elements differs from that of Ref. 7 only by 0.91%, and so good convergence can be expected.

The convergence studies for the composite plate are summarized in Tables 2 and 3, where the following material properties are used

Table 1 Convergence of critical force of isotropic plate ($a/b = 2$)

Poisson's ratio, ν	Number of elements 2×2	3×3	4×4	Ref. 7
0	161.3	112.6	110.8	109.8
0.3	154.4	107.2	105.8	——

Table 2 Convergence of free vibration frequencies of [15/− 15/15/− 15 deg] angle-ply laminated composite plate ($a/b = 1$, $a/h = 20$)

Number of elements	Bending mode number				
	1	2	3	4	5
1 × 1	7.63	9.89	23.50	25.46	37.07
2 × 2	6.50	9.76	19.77	20.47	31.73
3 × 3	6.49	9.68	17.91	20.29	31.47
4 × 4	6.48	9.65	17.89	20.12	31.18

Table 3 Convergence of critical force of laminated composite plate ($a/b = 1$, $a/h = 20$)

Plate, deg	Number of elements		
	2 × 2	3 × 3	4 × 4
[0/90/0/90]	82.1	79.5	79.7
[15/−15/15/−15]	88.9	81.3	80.2

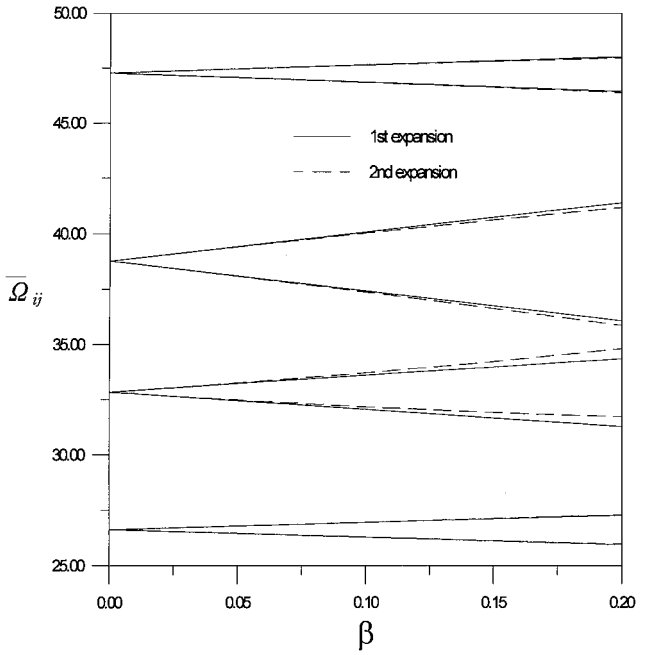

Fig. 2 Comparison of first and second expansion solutions for parametric instability ($\alpha = 0.1$, $\nu = 0.3$, $a/h = 10$, and $a/b = 0.5$).

in Ref. 18:

$$E_1/E_2 = 40, \qquad G_{12}/E_2 = G_{13}/E_2 = 0.5$$

$$G_{23}/E_2 = 0.6, \qquad \nu_{12} = 0.25$$

To the authors' knowledge, there has been no report on the dynamic stability of a completely free-edged composite plate under follower forces. Therefore, convergence was examined by the free vibration frequencies and critical forces. It can be seen from Table 2 that the natural frequencies show good convergence from 2 × 2 elements. Table 3 demonstrates the convergence characteristics of critical forces for the cross-ply and angle-ply laminate plates. The differences in critical forces between 3 × 3 elements and 4 × 4 elements are 0.3% (cross ply) and 1.4% (angle ply), respectively. Based on the preceding discussions and considering computation time, all further numerical results have been obtained with 4 × 4 elements for isotropic plates, and 3 × 3 elements for laminate composite plates.

Analysis of Isotropic Plates

Perturbation methods, including the method of multiple scales, are based on the assumption that coefficients of variables are sufficiently small in Ref. 17. Figure 2 compares the first- and second-order approximations of solutions given in Eq. (18). The expressions

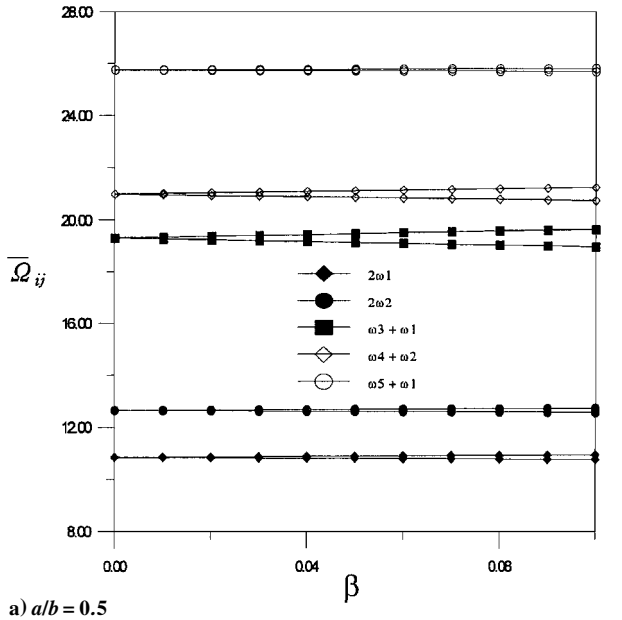

a) $a/b = 0.5$

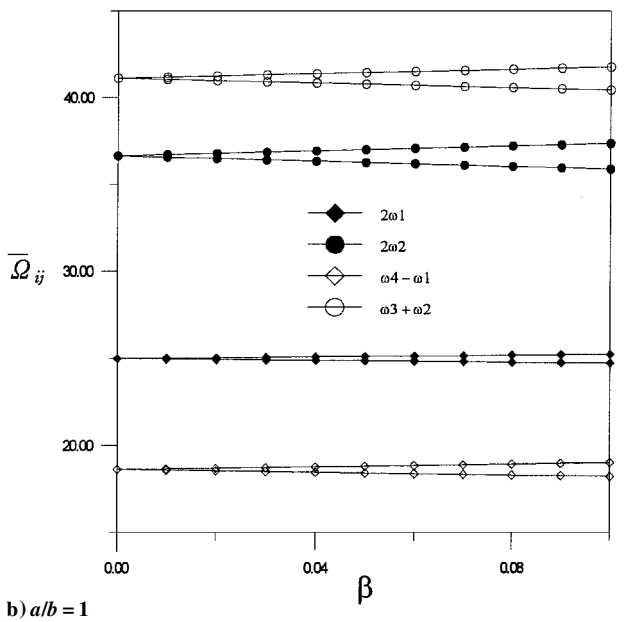

b) $a/b = 1$

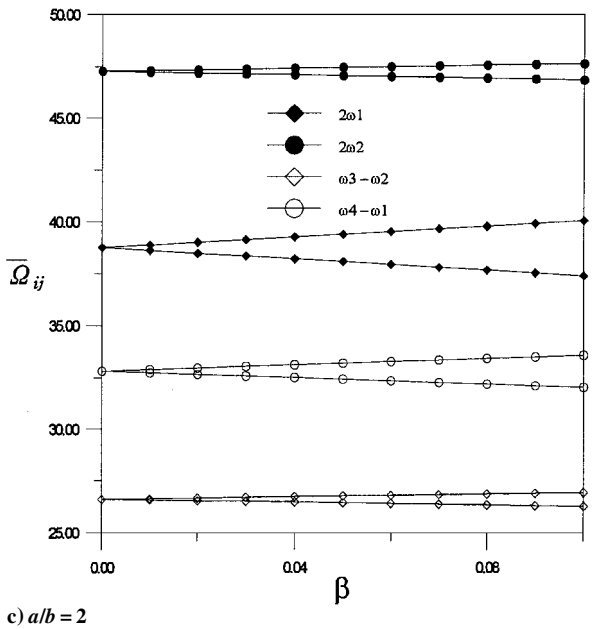

c) $a/b = 2$

Fig. 3 Parametric instability region of isotropic plate ($\alpha = 0.1$, $\nu = 0.3$, and $a/h = 10$).

for transition curves for the latter case can be found in Ref. 17. Solutions of the type $\Omega = \omega_q \pm \omega_p$ are chosen to determine the range of β for numerical calculation. From Fig. 2, it is easily seen that transition curves for the first- and second-order approximations show an insignificant difference for $0 < \beta < 0.1$. Furthermore, the two curves almost coincide with each other when the instability region is relatively narrow. As a result, we may restrict numerical studies to the region $0 < \beta < 0.1$ and can ensure the accuracy of results concerning the dynamic instability obtained by using the first-order approximation.

Figures 3a–3c show the dynamic instability regions for three aspect ratios, $a/b = 0.5$, 1, and 2. When $a/b = 0.5$, only sum-type combination resonances appear because R_{ij} and R_{ji} have the same signs. However, in the case $a/b = 1$, the instability region is observed near $\omega_4 - \omega_1$ also, indicating that combination resonances of sum and difference types exist simultaneously. Furthermore the combination resonance of a sum type due to the combination of different modes does not appear for $a/b = 2$. The dominant resonance types vary according to the aspect ratio. When $a/b = 0.5$, the instability region near $\omega_3 + \omega_1$ is wider than the others, whereas dominant regions are observed around $2\omega_2$ and $2\omega_1$ for $a/b = 1$ and 2, respectively. As shown in Ref. 6, for the critical forces of free-edged isotropic plates under constant follower forces, the combination-resonance types and instability regions are also very sensitive to the variation of aspect ratio when pulsating follower forces are applied to the plates.

Shapes of several vibration modes for the plate with $a/b = 2$ are plotted in Fig. 4. By comparison of Fig. 4 with the combination-resonance types of Fig. 3c, we see that the combination resonance occurs in the combinational form of only either symmetric (bending) modes (i.e., ω_2 and ω_3) or nonsymmetric (twisting) modes (i.e., ω_1 and ω_4) with respect to the center axis $y = b/2$ of the plate in the direction of force. Note that the combination resonances near $2\omega_i$, $i = 1, 2$, can also be considered one of the two combinations. It can be seen from Figs. 3a–3c that the combination resonances for $a/b = 0.5$ occur in different modes from those of $a/b = 1, 2$. This is because the third and fourth vibration modes are interchanged together as a/b is increased to 1 or 2. In all cases, the instability regions do not occur from the mixed combination of symmetric and nonsymmetric modes.

Practically, the platelike space structures may be modeled as isotropic plates with four free edges, and if the structures are constructed as a truss structure with a large member of frames, the Poisson ratio of the structures may be changed according to the array of frames. Figures 5a and 5b, together with Fig. 3c, illustrate the effect of the Poisson ratio ν on the dynamic instability.

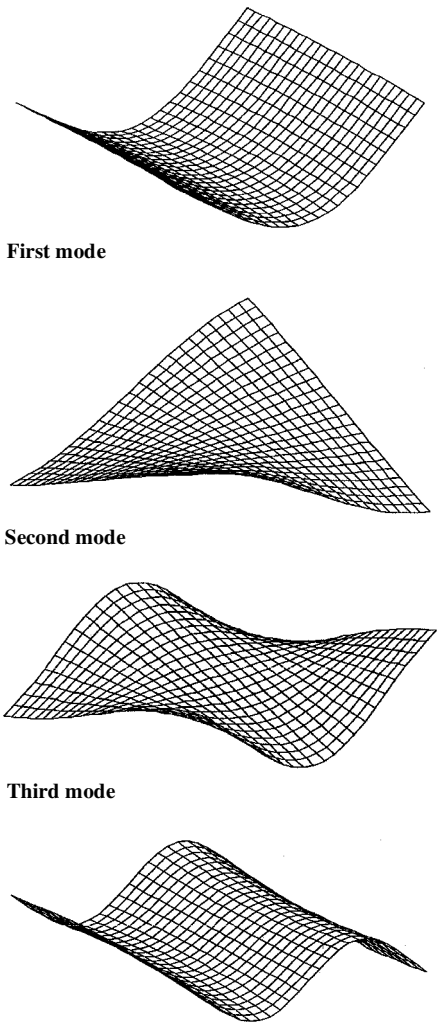

Fig. 4 Mode shape ($\alpha = 0.1$, $\nu = 0.3$, and $a/b = 2$).

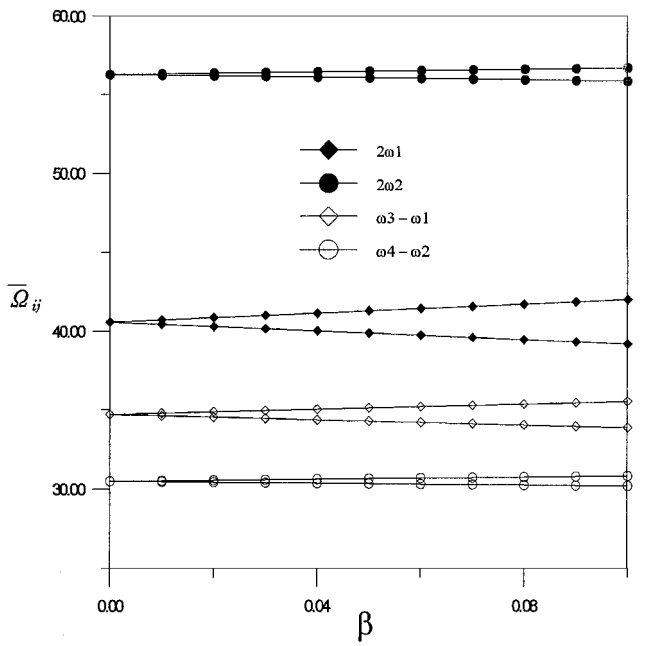

a) $\nu = 0$

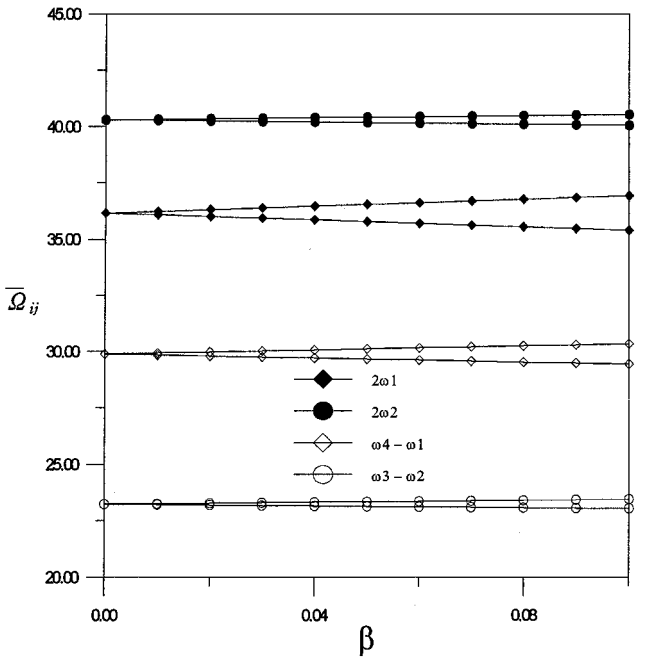

b) $\nu = 0.5$

Fig. 5 Parametric instability region of isotropic plate ($\alpha = 0.1$, $a/b = 2$, and $a/h = 10$).

The combination resonances take the same types for both $\nu = 0.3$ and 0.5. However, the instability regions move downwards while becoming narrower as ν increases from 0.3 to 0.5. When $\nu = 0$, the combination resonances take different forms, that is, the instability regions are generated near $\omega_3 - \omega_1$ and $\omega_4 - \omega_2$ whereas they appear around $\omega_4 - \omega_1$ and $\omega_3 - \omega_2$ for $\nu = 0.3$ and 0.5. As in the case of aspect ratio, this is due to the interchange of the third and fourth vibration modes with the increase of ν, and the variation of the Poisson ratio also does not alter the mode combinations and combination-resonance types.

The effects of rotary inertia and shear deformation on the dynamic instability are examined in Fig. 6 for the thickness ratios $h/a = \frac{1}{10}$ and $\frac{1}{100}$. As the thickness ratio increases, the instability regions shift downward while becoming narrower. Such effects are analyzed in further detail in Fig. 7. Because stability boundary curves expressed by the first-order approximation are linear, we can compute the variation of instability region using the following equation given in Ref. 14:

$$\bar{R}_{ij} = \left| \frac{\tilde{R}_{ij}\tilde{R}_{ji}}{\tilde{R}_s^2} \frac{\bar{\Omega}_s^2}{\bar{\Omega}_i \bar{\Omega}_j} \right|^{\frac{1}{2}} \tag{20}$$

where $\tilde{R}_s$ and $\bar{\Omega}_s$ are the reference values indicating the slopes of the instability regions near $2\omega_1$ for $\alpha = 0.1$ with $h/a = \frac{1}{100}$. The effects of rotary inertia and shear deformation remarkably appear when the thickness ratio exceeds $\frac{1}{20}$ and decrease the instability region that shows the stabilizing effect of rotary inertia and shear deformation.

Analysis of Composite Plate

This section analyzes the dynamic instability of the nonsymmetric composite plate with the same material properties as used in the convergence studies.

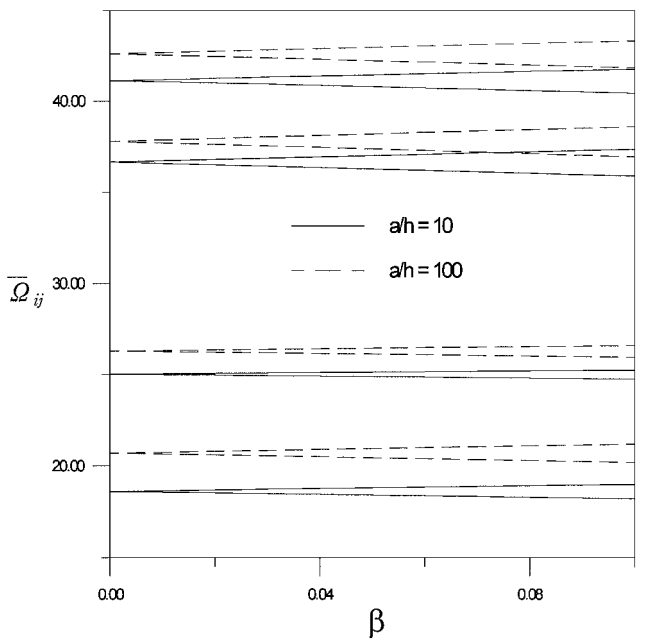

Fig. 6 Effect of thickness ratio on the parametric instability ($\alpha = 0.1$, $a/b = 1$, and $\nu = 0.3$).

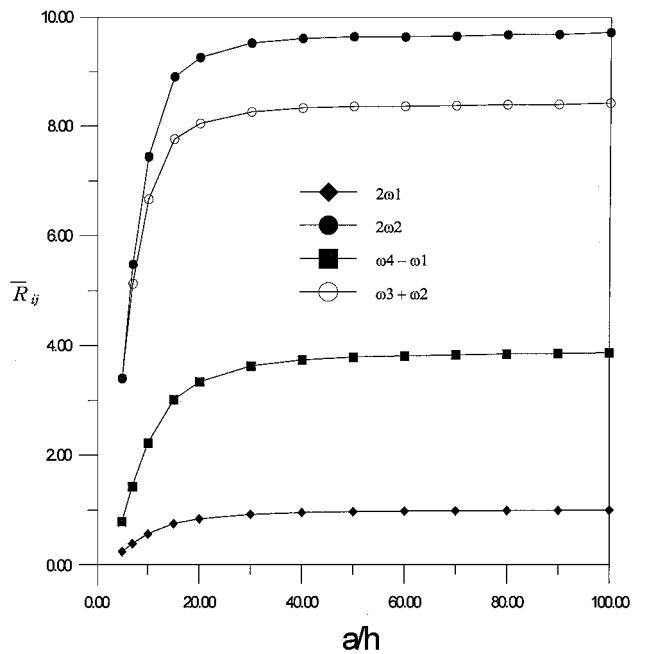

Fig. 7 Effects of rotary inertia and shear deformation on the parametric instability ($\alpha = 0.1$, $\nu = 0.3$, and $a/b = 1$).

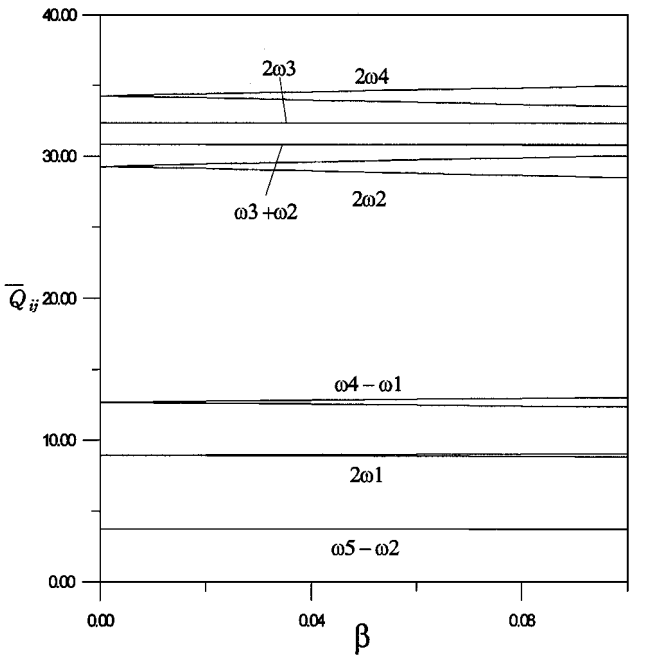

a) [0/90 deg]

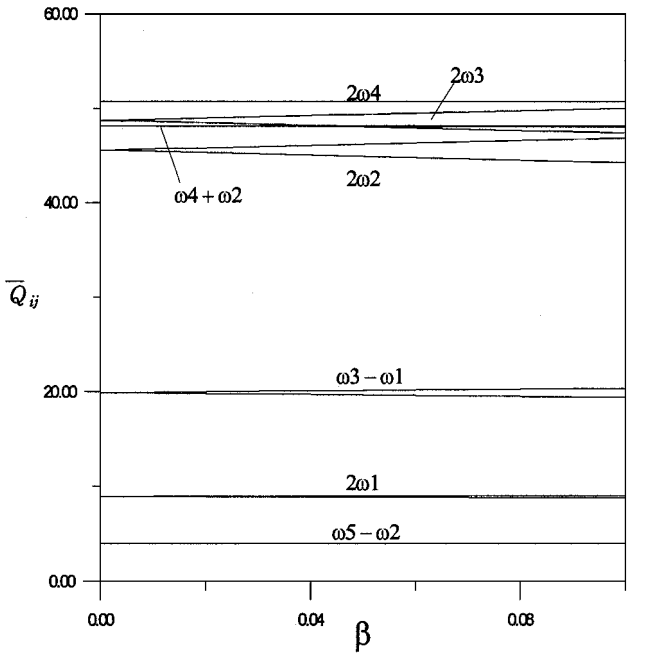

b) [0/90/0/90 deg]

Fig. 8 Parametric instability region of cross-ply laminated plate ($\alpha = 0.2$, $a/h = 20$, and $a/b = 1$).

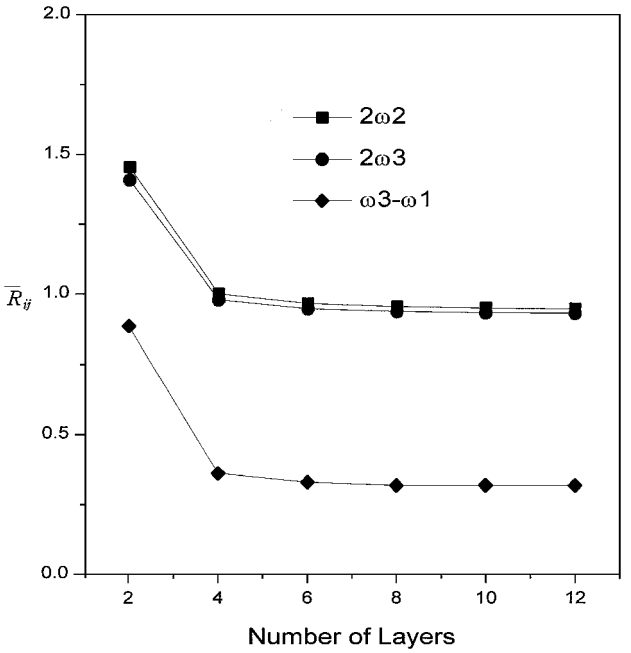

Fig. 9 Effect of the number of layers of cross-ply laminated plate on the parametric instability ($\alpha = 0.2, \bar{P}_{cr} = 79.5, a/h = 20$, and $a/b = 1$).

Figures 8a and 8b, respectively, illustrate the analysis results of the cross-ply composite plates with two and four layers. The instability regions show similar patterns except that the combination-resonance types of $\omega_4 - \omega_1$ and $\omega_3 + \omega_2$ in Fig. 8a are replaced by $\omega_3 - \omega_1$ and $\omega_4 + \omega_2$ of Fig. 8b. The replacement is the result of interchange between the third and fourth vibration modes as shown in the preceding section, and the mode combination types still remain the same. In both cases the dominant instability regions are observed near $2\omega_i$ and are concentrated between $2\omega_2$ and $2\omega_4$. The detail of the investigation on the effect of the number of layers is shown in Fig. 9, whose reference value is the width near $2\omega_2$ for $\alpha = 0.2$ with four layers. To compare the width of instability region under same magnitude of force, $\bar{P}_{cr}$ is fixed as the value of the four-layer case. It is seen that as the number of layers increase, the instability regions decrease. The smaller the number of layers there are, the bigger the effect of stretching–bending coupling is, so that the preceding result indicates that the stretching–bending coupling effect makes the instability region wide. In case of two layers, the mode combination discrepancy between Figs. 8a and 9 is also due to the interchange of the third and fourth vibration modes according to the P_0 magnitude (the difference of $\bar{P}_{cr}$ in the two cases leads to that of P_0). These results indicate that, for the cross-ply, nonsymmetric plate, the number of layers does not affect the combination-resonance types whereas it may affect the widths of the instability regions.

In Figs. 10a–10c, the effect of lamination angles on the variations of dynamic instability regions is studied for the angle-ply composite plates. It is found that the variation of lamination angles results in the change of combination-resonance types. Namely, only the sum-type combination resonances are observed in the [15/−15/15/−15 deg] angle-ply plate, whereas the difference-type $\omega_5 - \omega_3$ also appear for the [30/−30/30/−30 deg] angle-ply plate. Furthermore, the difference-type combination resonances are dominant over the sum-types in the [45/−45/45/−45 deg] angle-ply plate, implying that the difference-type combination resonances are the main causes of instability for large lamination angles. Note also that, contrary to the cross-ply plate, the widths of instability regions (except near $2\omega_3$ in Fig. 9b) do not show big differences from each other.

To investigate the effect of aspect ratio, the instability regions of a [15/−15/15/−15 deg] angle-ply plate with $a/b = 0.5$ and 2 are plotted in Figs. 11a and 11b, respectively. For $a/b = 0.5$, the combination-resonance types coincide with those of $a/b = 1$ (Fig. 8a), and the instability regions are concentrated between

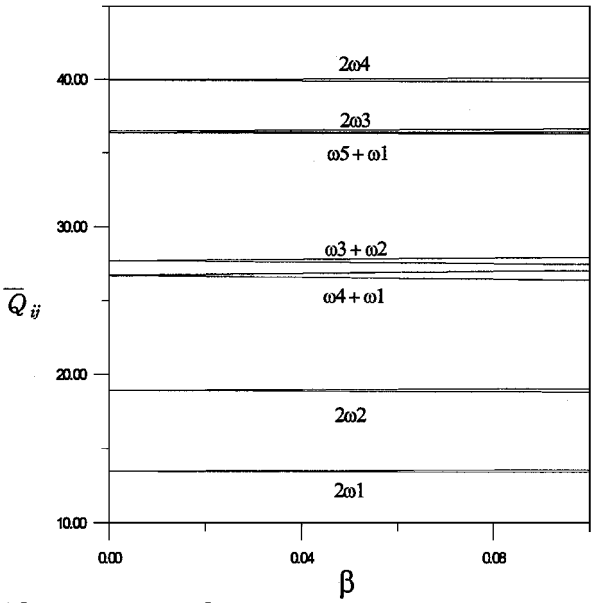

a) [15/− 15/15/− 15 deg]

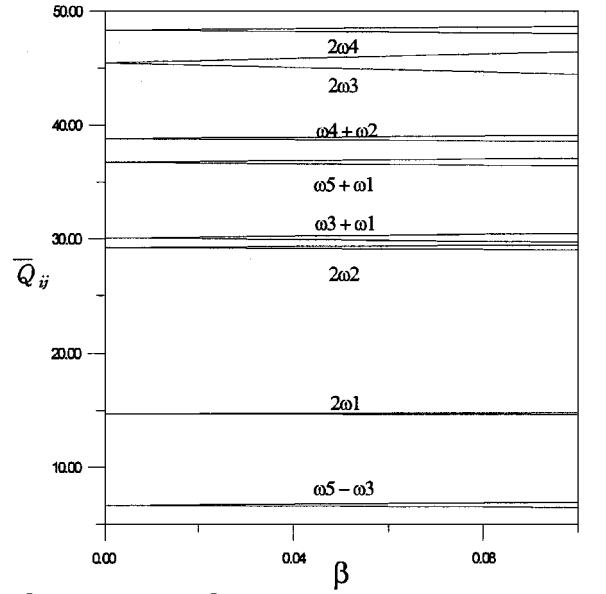

b) [30/− 30/30/− 30 deg]

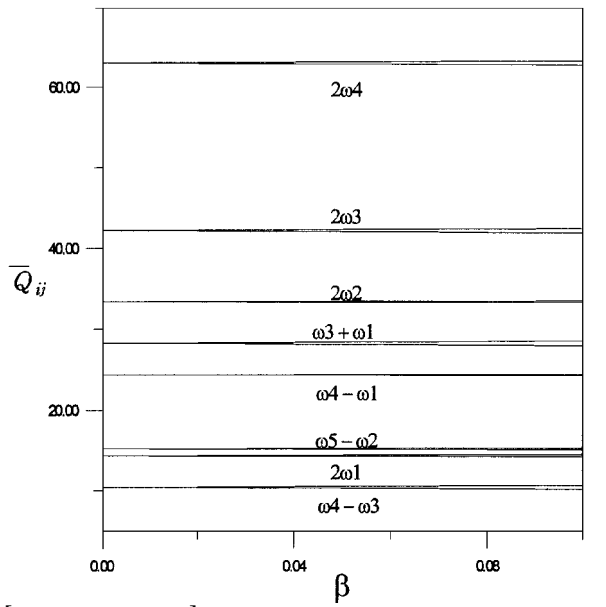

[45/− 45/45/− 45 deg]

Fig. 10 Parametric instability region of angle-ply laminated plate ($\alpha = 0.2, a/h = 20$, and $a/b = 1$).

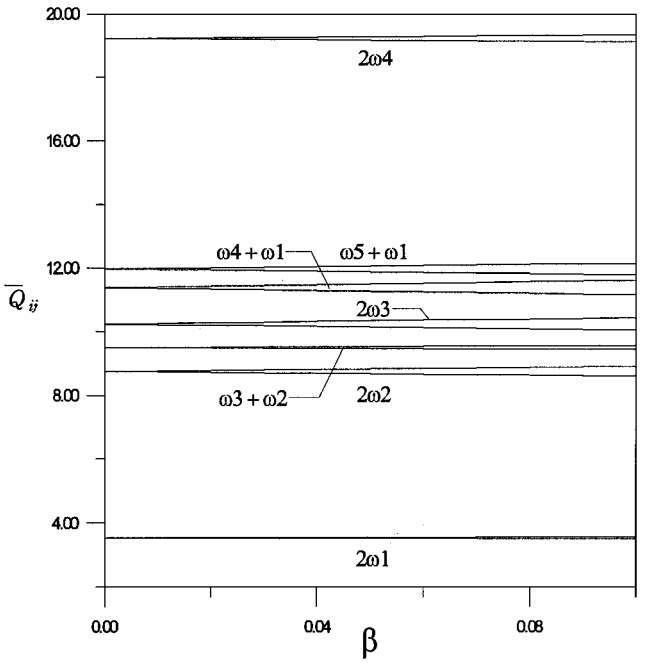

a) $a/b = 0.5$

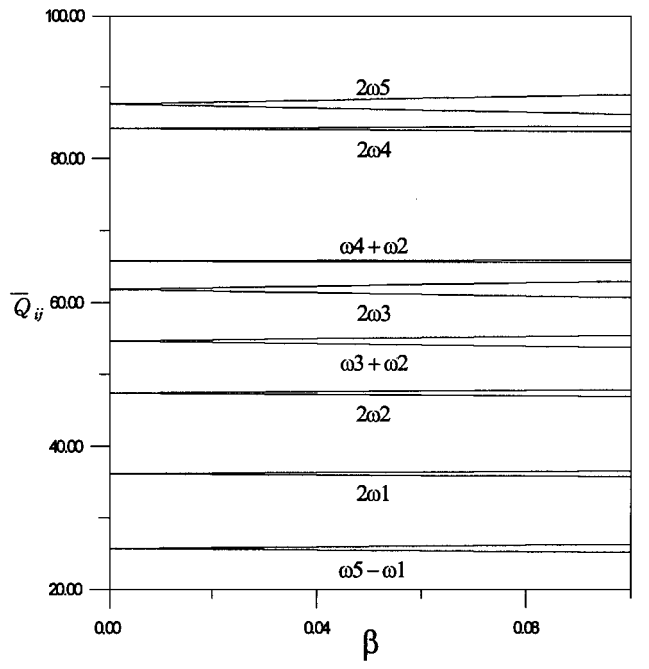

b) $a/b = 2$

Fig. 11 Parametric instability region of [15/− 15/15/− 15 deg] angle-ply laminated plate ($\alpha = 0.2$ and $a/h = 20$).

$\bar{\Omega} = 8 \sim 12$. As can be seen from Fig. 11b, the difference-type $\omega_5 - \omega_1$ appear for $a/b = 2$, but the sum types are still dominant. In contrast to the isotropic plate, the combination-resonance types are not sensitive to the variation of aspect ratio for the angle-ply, nonsymmetric composite plate.

Finally, we check, using the Eq. (20), the influence of thickness ratio on the dynamic instability regions in Fig. 12. As in the case of an isotropic plate (see Fig. 7), the whole instability regions become wider as the thickness ratio increases. However, the instability regions near $2\omega_2$ and $2\omega_4$ decrease in the range $h/a < \frac{1}{15}$. We can conclude from the discussions that the rotary inertia and shear deformation, which are more remarkable in the composite laminated plate than in the isotropic plate, have the effect of stabilizing the system.

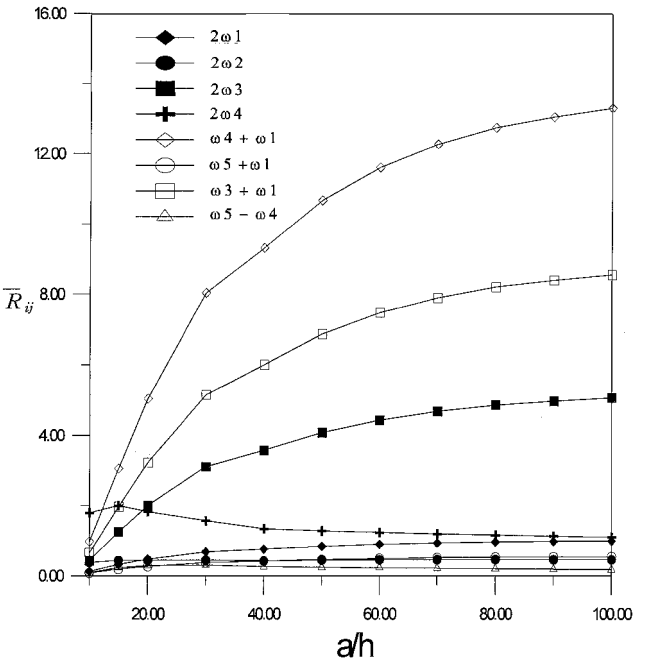

Fig. 12 Effects of rotary inertia and shear deformation on the parametric instability of [30/− 30/30/− 30 deg] angle-ply laminated plate ($\alpha = 0.05$ and $a/b = 1$).

Conclusions

The dynamic stability of a plate with four free edges subjected to pulsating follower forces was studied. The discretized equation of motion was obtained by the finite element method, and then the method of multiple scales was used to investigate the dynamic instability region. The conclusions obtained can be summarized as follows:

1) The combination resonances occur in the combinational form of only either symmetric or nonsymmetric modes with respect to the center axis $y = b/2$ of the plate in the direction of force.

2) For the isotropic plate, the aspect ratio sensitively affect the types and widths of combination resonances. However, the variation of the Poisson ratio does not change the combination-resonance types.

3) For the nonsymmetric, cross-ply composite plate, the number of layers alters the widths of instability regions, but it does not influence the combination-resonance types. Contrary to the isotropic plate, the variation of aspect ratio has no sensitive effect on the combination-resonance types for the angle-ply composite plate. Instead, the variation of lamination angle is the main factor causing the change in combination-resonance types. As the lamination angle increases, the difference-type combination resonances become dominant over the sum types.

4) The rotary inertia and shear deformation stabilizes the system by reducing the instability regions that can be observed more readily in the composite plate than in the isotropic plate.

Acknowledgment

The authors thank the Korea Science and Engineering Foundation for financial support via Research Project 961-1002-017-2.

References

[1] Beal, T. R., "Dynamic Stability of a Flexible Missile Under Constant and Pulsating Thrusts," *AIAA Journal*, Vol. 3, No. 3, 1965, pp. 486–494.

[2] Wu, J. J., "On Missile Stability," *Journal of Sound and Vibration*, Vol. 49, No. 1, 1976, pp. 141–147.

[3] Park, Y. P., "Dynamic Stability of a Free Timoshenko Beam Under a Controlled Follower Force," *Journal of Sound and Vibration*, Vol. 113, No. 3, 1987, pp. 407–415.

[4] Park, Y. P., and Mote, C. D., Jr., "The Maximum Controlled Follower Force on a Free-Free Beam Carrying a Concentrated Mass," *Journal of Sound and Vibration*, Vol. 98, No. 2, 1985, pp. 247–256.

[5] Sugiyama, Y., Matsyike, J., Ryu, B. J., Katayama, K., Kinoi, S., and Enomoto, N., "Effect of Concentrated Mass on Stability of Cantilevers Under Rocket Thrust," *AIAA Journal*, Vol. 33, No. 3, 1995, pp. 499–503.

[6]Higuchi, K., and Dowell, E. H., "Dynamic Stability of a Rectangular Plate with Four Free Edges Subjected to a Follower Force," *AIAA Journal*, Vol. 28, No. 7, 1990, pp. 1300–1305.

[7]Higuchi, K., and Dowell, E. H., "Effects of the Poisson Ratio and Negative Thrust of the Dynamic Stability of a Free Plate Subjected to a Follower Force," *Journal of Sound and Vibration*, Vol. 129, No. 2, 1989, pp. 255–269.

[8]Hutt, J. M., Asce, A. M., and Salam, E., "Dynamic Stability of Plates by Finite Elements," *Journal of the Engineering Mechanics Division, ASCE*, Vol. 97, No. EM3, 1971, pp. 879–899.

[9]Duffield, R. C., and Willems, N., "Parametric Resonance of Stiffened Rectangular Plates," *Journal of Applied Mechanics*, Vol. 39, No. 1, 1972, pp. 217–226.

[10]Young, T. H., and Chen, F. Y., "Stability of Fluttered Panels Subjected to In-Plane Harmonic Forces," *AIAA Journal*, Vol. 31, No. 9, 1993, pp. 1667–1673.

[11]Young, T. H., and Chen, F. Y., "Stability of Skew Plates Subjected to Aerodynamic and In-Plane Forces," *Journal of Sound and Vibration*, Vol. 171, No. 5, 1994, pp. 603–615.

[12]Srinivasan, R. S., "Dynamic Stability of Rectangular Laminated Composite Plates," *Computers and Structures*, Vol. 24, No. 2, 1986, pp. 233–238.

[13]Chen, L. W., and Yang, J. Y., "Dynamic Stability of Laminated Composite Plates by the Finite Element Method," *Computers and Structures*, Vol. 36, No. 5, 1990, pp. 845–851.

[14]Cederbaum, G., "Dynamic Instability of Shear Deformable Laminated Plates," *AIAA Journal*, Vol. 29, No. 11, 1991, pp. 2000–2005.

[15]Liao, C. L., and Cheng, C. R., "Dynamic Stability of Stiffened Laminated Composite Plates and Shells Subjected to In-Plane Pulsating Forces," *Journal of Sound and Vibration*, Vol. 174, No. 3, 1994, pp. 335–351.

[16]Dhatt, G., and Touzot, G., *The Finite Element Method Displayed*, Wiley, New York, 1984.

[17]Nayfeh, A. H., and Mook, D. T., *Nonlinear Oscillations*, Wiley, New York, 1979.

[18]Jones, R. M., *Mechanics of Composite Materials*, Scripta, Washington, DC, 1975.

G. A. Kardomateas
Associate Editor